Divacancy and resistivity profiles in n-type Si implanted with 1.15-MeV protons

H. Kauppinen and C. Corbel
Institut National des Sciences et Techniques Nucléaires, Centre d'Etudes Nucléaires de Saclay, 91191 Gif-sur-Yvette Cedex, France

K. Skog, K. Saarinen, T. Laine, and P. Hautojärvi
Laboratory of Physics, Helsinki University of Technology, 02150 Espoo, Finland

P. Desgardin and E. Ntsoenzok
CERI-CNRS, 3A rue de la Férollerie, 45071 Orléans Cedex 2, France
(Received 25 October 1996)

Defect profiles were determined in proton-implanted low-doped ([P]=1×10^{14} cm^{-3}) n-type silicon layers by performing positron-electron pair momentum-distribution measurements with a slow-positron beam, conventional positron lifetime, and e^+-e^- pair momentum-distribution measurements with a ^{22}Na-source and spreading resistance measurements. The dominant positron trap induced by 1.15 and 3.0 MeV proton implantations is the silicon divacancy V_2. Compared to the values in bulk, the characteristic positron lifetime and the characteristic low- and high-momentum parameters of the e^+-e^- pair momentum distribution at the divacancy are $\tau_d=300$ ps$=1.35\tau_b$, $S_d=1.052S_b$, and $W_d=0.78W_b$, respectively. The divacancy is observed in the negative charge state V_2^-. The divacancy profile is determined in n-type Si implanted with 1.15-MeV (20 μm) protons to a dose 1×10^{14} cm^{-2} and the maximum concentration $[V_2^-]=4-8\times10^{15}$ cm^{-3} is observed at depths 16–18 μm. The resistivity increases with increasing divacancy concentration. After annealing at 400 °C the spreading resistance measurements reveal a region of shallow hydrogen-related donors at depths 15–21 μm. The positron annihilation results support the idea that the introduction of shallow donors is due to the formation of hydrogen-vacancy complexes during the annealing. [S0163-1829(97)08216-7]

I. INTRODUCTION

Proton implantation can be used for controlling the minority carrier lifetime in silicon power devices. The implantation-induced defects in silicon serve as recombination centers and reduce the free-carrier lifetime in the device.[1] As a charged heavy particle the implanted proton has a well-defined stopping range in the target material. The defect layer induced by proton implantation is therefore well localized, in contrast with defect distributions introduced by electron irradiation or by conventional gold or platinium diffusion.

The performance of the proton-implanted silicon device depends strongly on the implantation-induced defects. The defects are often electrically active and have deep electron levels in the band gap of silicon. In low-dose implantations capacitance measurements have been used to determine the deep electron levels. For example, deep-level-transient spectroscopy (DLTS) measurements in a silicon p-n diode implanted with 1.5 MeV protons to a dose 5×10^{10} cm^{-2} reveal an acceptor level at $E_c-0.42$ eV, where E_c is the energy at the bottom of the conduction band.[2] This deep level seems to be the dominant recombination center and it is attributed to the divacancy. When low-doped silicon is implanted to a high proton dose ($\geq10^{14}$ cm^{-2}) the material becomes electrically compensated and highly resistive. This can be observed, e.g., by spreading resistance measurements.

The proton-implanted silicon device often requires an annealing stage during the packaging. Then the device behavior is determined by the defects remaining after the annealing. An interesting phenomenon related to the annealing is that proton implantation and subsequent thermal annealing at 300–500 °C introduces hydrogen-related shallow donors at $E_c-0.026$ eV in silicon.[3,4] If the concentration of these donors is not negligible compared to the dopant concentration, the donors can be harmful for the device performance, for example, by lowering the breakdown voltage of the device.

In order to understand the emergence of the deep levels and the electrical properties of the implanted material it is important to know the atomic structure of the defects. Positron-annihilation spectroscopy can be used for studying vacancy-type and negative ion-type defects in semiconductors.[5–7] The positron lifetime and the momentum distribution of the annihilating positron-electron pair depends on the annihilation state of the positron. Positron trapping at vacancy defects is manifested as an increase of the positron lifetime with respect to the positron lifetime in the lattice and as a narrowing of the e^+-e^- pair momentum distribution with respect to the momentum distribution in the lattice. Ion-type defects can trap positrons at low temperatures and the corresponding annihilation state is close to the free-annihilation state in the lattice.

In previous positron-annihilation studies, e^+-e^- pair momentum-distribution measurements with a slow-positron beam have been performed in silicon implanted with various proton energies: 15.5 keV (77 and 300 K, Brusa *et al.*[8]), 30, 60, and 100 keV (300 K, Keinonen *et al.*[9]). In these studies a localized divacancy layer near the surface was observed and the absence of positron trapping at vacancies near the proton range can be explained by the formation of hydrogen-vacancy complexes escaping the positron detection. In the study of Goldberg, Schultz, and Simpson[10] variously doped

0163-1829/97/55(15)/9598(11)/$10.00 © 1997 The American Physical Society

TABLE I. n-type Si(P) samples prepared for slow-positron, fast-positron, and spreading resistance measurements. The proton implantations were performed at three different runs. Samples $A1_{a-h}$, $A2$, and $A5$ have been thermally annealed at 400 °C during 5 min after the proton implantation. Samples $R1_{a-d}$, $H1_{a-i}$, and $A1_{a-h}$ prepared for slow-positron measurements have been chemically etched at different depths. The etched depths x_{etch} are indicated by the subscripts: a, b, c, and $d=0$, 6, 9.5, and 14.8 μm for as-grown samples $R1_{a-d}$, a, b, c, d, e, f, g, h, and $i=0$, 5, 10, 14.5, 17, 19, 20, 23, and 25 μm for proton-implanted samples $H1_{a-i}$, and a, b, c, d, e, f, g, and $h=0$, 4, 5, 9, 13, 15, 16.5, and 22 μm for proton-implanted and annealed samples $A1_{a-h}$.

Measurement technique	Unimplanted reference samples	Proton implantation					
		Run	Energy (MeV)	Range (μm)	Dose (cm^{-2})	As-implanted samples	Annealed samples
Slow positrons	$R1_a$, $R1_b$, $R1_c$, $R1_d$	1	1.15	20	1×10^{14}	$H1_a$, $H1_b$,...,$H1_i$	$A1_a$, $A1_b$,...,$A1_h$
		2	1.15	20	1×10^{14}	$H2$	$A2$
Fast positrons	$R2$	2	3.0	90	1×10^{14}	$H3$	
		2	3.0	90	8×10^{14}	$H4$	
Spreading resistance	$R5$	3	1.15	20	1×10^{14}	$H5$	$A5$

Si samples were implanted with 1.0- and 2.6-MeV (77 K) protons and the saturation of the divacancy formation was studied with a slow-positron beam. Higher proton implantation energies have been used in positron lifetime measurements with a ^{22}Na positron source. Mäkinen, Rajainmäki, and Linderoth[11,12] studied silicon implanted with 7 MeV (15 K) protons and irradiated with 12 MeV protons (15 K). The observed annealing stages were attributed to monovacancies, oxygen-vacancy complexes, and hydrogen-vacancy complexes.

Our objective in this work is to correlate vacancy and resistivity profiles in room-temperature proton-implanted lightly n-type chemically vapor deposited (CVD) Si(P) layers, before and after 5 min. annealing at 400 °C. We concentrate on layers where the proton range is either 20 μm (1.15 MeV) or 90 μm (3.0 MeV) and where capacitance measurements are impossible due to the compensation by implantation.

The vacancy profile along the proton track is obtained in a set of layers which, after 1.15 MeV proton implantations in similar conditions, have been chemically etched at different depths from 0 to 25 μm. The implantation-induced vacancies are detected by measuring the e^+-e^- pair momentum distribution via the Doppler-broadening of the 511-keV annihilation line. The Doppler broadening is measured in each etched layer with a slow-positron beam that allows us to vary the mean positron-implantation depth from 0 to 3 μm. The resistivity profiles after 1.15 MeV proton implantation are obtained with spreading resistance measurements.

In order to determine the nature and the charge state of the defects we performed positron lifetime and Doppler-broadening measurements with a ^{22}Na positron source in n-type Si layers implanted with 1.15- and 3.0-MeV protons. Positrons scan then the whole proton track because they are implanted from the surface to a mean penetration depth of about 100 μm.

II. EXPERIMENT

A. Samples

The proton-implanted silicon layers were 90 μm thick, (111) oriented, and doped with phosphorus $[\mathrm{P}]=1\times10^{14}\,\mathrm{cm}^{-3}$. The layers were CVD grown on a n^+-type Czochralski-silicon substrate. As shown in Table I, the implantations were performed at 300 K with proton energies 1.15 MeV (20 μm) and 3.0 MeV (90 μm) at three separate runs. Twenty-one layers $H1_{a-i}$, $H2$, $H5$, $A1_{a-h}$, $A2$, and $A5$ were implanted with 1.15 MeV protons to a dose $1\times10^{14}\,\mathrm{cm}^{-2}$. Layers $A1_{a-h}$, $A2$, and $A5$ were subsequently annealed at 400 °C during 5 min. Two layers, $H3$ and $H4$, were implanted with 3.0 MeV protons to doses 1×10^{14} and $8\times10^{14}\,\mathrm{cm}^{-2}$, respectively. Layers $R1_{a-d}$, $R2$, and $R5$ are unimplanted reference samples.

B. Profiling measurements with slow positrons and spreading resistance

For the vacancy profiling, layers $H1_{a-i}$, $A1_{a-h}$, and $R1_{a-d}$ were chemically etched in a solution of HF and $\mathrm{HNO_3}$ in order to remove different depths x_{etch} of material. The etched depths were measured with a Rank-Taylor Talysurf 10 profiler and they are indicated in Table I. After etching, these layers were subjected to Doppler-broadening measurements with a slow-positron beam at 300 K. The Doppler-broadening ΔE_γ of the annihilation line at 511 keV is related to the momentum of the annihilating e^+-e^- pair by $\Delta E_\gamma = p_z/2c$, where p_z is the momentum component along the line of emission of the two annihilation gamma rays.

The Doppler-broadened annihilation line $I(E_\gamma)$ at 511 keV was measured as a function of the incident positron energy. By scanning the energy of the monoenergetic ($\delta E \leqslant 3$ eV) positron beam from 0.5 to 24 keV, the mean positron-penetration depth was changed from 4 nm to 3 μm. At each incident positron energy, the annihilation line $I(E_\gamma)$, containing 2×10^6 counts, was recorded with a high purity (HP) germanium detector with an energy resolution of 1.2 keV. The shape of the e^+-e^- pair momentum distribution is characterized by the low-momentum parameter S and the high-momentum parameter W, defined as the ratios $S = N_S/N_{\mathrm{TOT}}$ and $W=(N_{W1}+N_{W2})/N_{\mathrm{TOT}}$, respectively. The integral N_S is the area of the central region [511−0.7, 511+0.7] keV of the annihilation peak, N_{W1} and N_{W2} are areas of the wing regions [511−5.1, 511−2.8] keV and [511+2.8, 511+5.1] keV, respectively, and N_{TOT} is the total area of the annihilation peak in the region [511−6.4, 511+6.4] keV. Thus, S and W parameters are the fractions of positrons an-

nihilating with electrons in the low-momentum range $p_z = (0-2.8)\times 10^{-3} m_0 c$ and in the high-momentum range $p_z = (11-20)\times 10^{-3} m_0 c$, respectively.

Doppler-broadening measurements with the slow-positron beam at the surfaces (0–3 μm) of layers $H1_{a-i}$, give the defect profile induced by the 1.15 MeV proton implantation. Measurements in layers $A1_{a-h}$ give the defect profile after implantation and annealing at 400 °C. Layers $R1_{a-d}$ are measured in order to monitor the effect of the etching on the sample surface.

For resistivity profiling, we measured the spreading resistance at 300 K at depths 0–30 μm below the layer surface in layers $H5$, $A5$, and $R5$.

C. Bulk measurements with fast positrons from a ^{22}Na source

Positron lifetime and Doppler-broadening measurements were carried out as a function of temperature for the as-grown layer $R2$, for the 1.15-MeV (20 μm) proton-implanted layers $H2$ and $A2$ and for the 3.0-MeV (90 μm) proton-implanted layers $H3$ and $H4$. In the proton-implanted layers the positron lifetime spectra can be decomposed to free and defect-related annihilation states, which enables us to determine the characteristic positron lifetime and the characteristic momentum parameters S and W of the implantation-induced defects.

The positron source was 60 μCi of β^+-active ^{22}NaCl deposited on a 5-μm Al foil. The source was sandwiched between two identical pieces of the sample and the sandwich was mounted in a cryostat. The temperature of the sample was scanned between 30 and 300 K, with 20-K steps. At each temperature the positron lifetime spectrum and the Doppler-broadened annihilation line at 511 keV were recorded, containing 2×10^6 and 5×10^6 counts in the peaks, respectively. The time resolution of the lifetime spectrometer was 225 ps. The source was found to contribute to the measured lifetime spectra with 230- and 500-ps components, corresponding to annihilations in the Al foil and in the NaCl salt, respectively. In addition a long component of 1500 ps, related to positronium formation in the source-sample system, was observed. The corresponding intensities 5.4%, 0.8%, and 0.15%, respectively, were subtracted from the spectra before further analysis. In the Doppler-broadening experiments, the resolution of the HP Ge detector and the definitions of the S and W parameters are the same as in the slow-positron experiments.

III. RESULTS

A. Slow-positron measurements at 300 K

Figure 1 illustrates the typical behavior of the measured low-momentum parameter S as a function of the incident slow-positron energy. The shapes of the $S(E)$ curves in Fig. 1 show similar features in all measured layers: $S(E)$ increases strongly from 0.5 to 10 keV and tends to level at energies higher than 15 keV. Also the $W(E)$ curves behave in a similar way in all measured layers: the $W(E)$ curves decrease strongly from 0.5 to 10 keV and tend to level at energies higher than 15 keV. The leveling indicates that in terms of positron annihilation states the layers are relatively homogeneous. The strong changes of the $S(E)$ and $W(E)$ curves at small incident energies can be understood to result from the positron diffusion to the surface. We can describe the $S(E)$ and $W(E)$ curves as

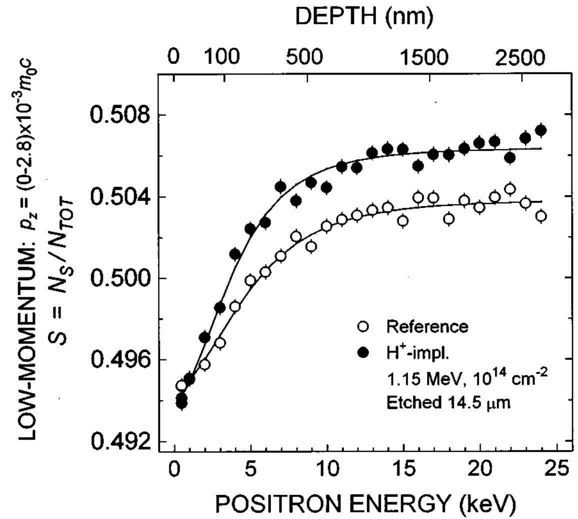

FIG. 1. Low-momentum parameter S of the Doppler-broadened annihilation line measured at 300 K vs incident positron energy in as-grown (sample $R1_a$) and in proton-implanted (sample $H1_d$) n-type Si. The solid lines are fits of Eq. (1a) in the data.

$$S(E) = \eta_{\rm surf}(E) S_{\rm surf} + \eta_{\rm in}(E) S_{\rm in}, \tag{1a}$$

$$W(E) = \eta_{\rm surf}(E) W_{\rm surf} + \eta_{\rm in}(E) W_{\rm in}, \tag{1b}$$

where $S_{\rm surf}$ and $W_{\rm surf}$ are the values of S and W at the surface, $S_{\rm in}$ and $W_{\rm in}$ are the values inside the layer below the etched surface, and $\eta_{\rm surf}(E)$ and $\eta_{\rm in}(E)$ are the fractions of positrons annihilating at the surface and in the layer, respectively.

The motion of the positron in steady state is described by the diffusion-annihilation equation[9,13]

$$D_+ \nabla^2 n(x,E) - (\lambda_b + \kappa) n(x,E) + P(x,E) = 0, \tag{2}$$

where $n(x,E)$ is the stationary positron density at depth x and at incident positron energy E, D_+ is the positron-diffusion coefficient, λ_b is the positron annihilation rate in the silicon lattice, κ is the positron trapping rate to defects in the layer, and $P(x,E)$ is the positron implantation-rate profile. As the implantation-rate profile we use a Makhovian distribution[14,15]

$$P(x,E) = -\frac{d}{dx} \exp[-(x/x_0)^m], \tag{3}$$

where the parameter x_0 is proportional to the mean positron-implantation depth $\bar{x} = 0.886 x_0 = (A/\rho)[E(\mathrm{keV})]^n$. The density of silicon is $\rho = 2.33$ g/cm^3 and we use the implantation parameters $A = 2.95$ μg/cm^2, $n = 1.7$, and $m = 1.9$.[16,17] The annihilation fractions $\eta_{\rm surf}$ and $\eta_{\rm in}$ in Eqs. (1a) and (1b) are integrals of the first and second term in Eq. (2), respectively. The fitting of Eqs. (1a) and (1b) in our data was carried out iteratively by using VEPFIT.[18] The adjusted parameters in the fitting procedure were $S_{\rm in}$, $S_{\rm surf}$, $W_{\rm in}$, $W_{\rm surf}$ and the so-called effective diffusion length $L_{\rm eff} = \sqrt{D_+/(\lambda_b + \kappa)}$.

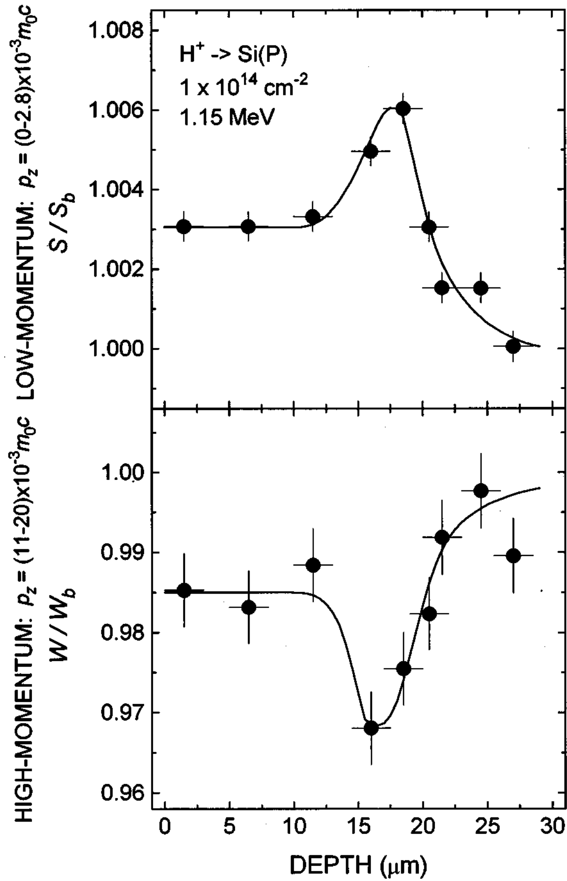

FIG. 2. Results of the fittings of Eq. (1a) in S data and Eq. (1b) in W data. The S and W data were measured at 300 K in 1.15-MeV proton-implanted n-type Si (samples $H1_{a-i}$) at different etched depths. The solid lines are guides to the eye.

In the as-grown n-type Si layers $R1_{a-d}$ the parameters $S_{\rm in}$ and $W_{\rm in}$ were found to be constant and are taken as reference values: $S_{\rm ref}=0.5039\pm0.0001$, $W_{\rm ref}=0.020\,45\pm0.000\,07$. Also the diffusion length was constant $L_{\rm eff}=(220\pm10)$ nm in samples $R1_{a-d}$. The surface parameters were found to vary randomly as $S_{\rm surf}=0.478-0.499$ and $W_{\rm surf}=0.0256-0.0278$.

In the proton-implanted layers $H1_{a-i}$ (1.15 MeV, 20 μm, 1×10^{14} cm^{-2}) the $S_{\rm in}$ and $W_{\rm in}$ characterize the positron annihilation states in the regions $[x_{\rm etch},x_{\rm etch}+3\ \mu{\rm m}]$, where $x_{\rm etch}$ is the etched depth and 3 μm is the maximum mean positron-implantation depth obtained with the maximum incident energy $E=24$ keV. In Fig. 2 the data points $S=S_{\rm in}(x_{\rm etch})$ and $W=W_{\rm in}(x_{\rm etch})$ are drawn in the middle of these 3-μm regions, i.e., at depth$=x_{\rm etch}+1.5$ μm, and they are normalized to the values S_b and W_b, respectively, in the Si lattice (see Sec IV A 1). We see that at depths 0–14 μm S (W) is constant and higher (lower) than in as-grown n-type Si. At depths 14–20 μm there is a peak in both S and W profiles. The tails of the profiles extend to 25–28 μm where S and W approach the corresponding values in as-grown n-type Si.

In layers $A1_{a-h}$ annealed at 400 °C $S_{\rm in}$ and $W_{\rm in}$ were found to be the same as in as-grown n-type Si, at depths 0–25 μm.

B. Fast-positron measurements

1. Positron lifetime measurements

In the as-grown n-type Si layer $R2$ one lifetime component was sufficient to describe the positron lifetime spectra at 30–300 K. The measured positron lifetime $\tau_{\rm ref}$ is 221 ps at 30 K and 222 ps at 300 K. At intermediate temperatures the positron lifetime depends linearly on the measurement temperature. In the n^+-type substrate the positron lifetime was the same as in the n-type Si layer.

To analyze correctly the positron lifetime spectra in the proton-implanted layers $H2$, $H3$, and $H4$, we need to consider the proton range in the layers. Figure 2 shows that the 1.15-MeV (20 μm) proton-implanted layer is virtually unaffected by the proton implantation at depths >25 μm. This unimplanted region, consisting of as-grown n-type Si and the n^+-type Si substrate, is characterized by the positron lifetime $\tau_{\rm ref}$. In the implanted region at 0–25 μm the positron lifetime is defined as $\tau_{\rm impl}$. Similarly, in the 3.0-MeV (90 μm) proton-implanted layers $H3$ and $H4$ an unimplanted region at depths >95 μm is characterized by the positron lifetime $\tau_{\rm ref}$ and in a proton-implanted region at 0–95 μm the positron lifetime is $\tau_{\rm impl}$.

As mentioned above, the thermal positron diffusion length $L_{\rm ref}$ in as-grown n-type Si is 220 nm at 300 K. Hence, the fractions of positrons annihilating in the proton-implanted and unimplanted regions can be calculated from the stopping distribution $P(x)=\alpha\exp(-\alpha x)$ of β^+ particles in Si. For a ^{22}Na source and Si we use a characteristic penetration depth $1/\alpha=110$ μm.[19] The fractions of positrons annihilating in the unimplanted regions are then $I_{\rm ref}=80\%$ in the 1.15-MeV (20 μm) proton-implanted layer $H2$ and $I_{\rm ref}=42\%$ in the 3.0-MeV (90 μm) proton-implanted layers $H3$ and $H4$.

A three-component model function $-dn/dt=(I_1/\tau_1)\exp(-t/\tau_1)+(I_2/\tau_2)\exp(-t/\tau_2)+(I_{\rm ref}/\tau_{\rm ref})\exp(-t/\tau_{\rm ref})$ was fitted in the positron lifetime spectra measured in the proton-implanted layers. The proton-implanted region is characterized by the two former exponential terms. The fitting parameters $I_{\rm ref}$ and $\tau_{\rm ref}$ in the unimplanted region are constrained to the fixed values given above. The average positron lifetime in the sample is defined as

$$\tau_{\rm ave}=I_1\tau_1+I_2\tau_2+I_{\rm ref}\tau_{\rm ref}=(1-I_{\rm ref})\tau_{\rm impl}+I_{\rm ref}\tau_{\rm ref},\qquad(4)$$

where $\tau_{\rm impl}=(I_1\tau_1+I_2\tau_2)/(I_1+I_2)$ is the positron lifetime in the proton-implanted region.

As shown in Fig. 3, in the proton-implanted layer $H2$ (1.15 MeV, 20 μm, 1×10^{14} cm^{-2}) the average positron lifetime $\tau_{\rm ave}$ is above $\tau_{\rm ref}$ at 30–300 K and increases with decreasing temperature. The second lifetime component in layer $H2$ is constant, $\tau_2=(300\pm10)$ ps, throughout the temperature range 30–300 K. Also in layer $H4$ (3.0 MeV, 90 μm, 8×10^{14} cm^{-2}) we observe in Fig. 3 that $\tau_{\rm ave}$ is above $\tau_{\rm ref}$ at 30–300 K and increases with decreasing temperature. The second lifetime component in layer $H4$ is constant, $\tau_2=(300\pm5)$ ps at 110–300 K, and decreases from 300 to 280 ps as temperature decreases from 110 to 30 K. In layer $H3$ (3.0 MeV, 90 μm, 1×10^{14} cm^{-2}) the positron lifetime results are similar to those in layers $H2$ and $H4$. The average positron lifetime $\tau_{\rm ave}$ is 227 ps at 300 K, 234 ps at 110 K, and 237 ps at 30 K. The second lifetime component in layer

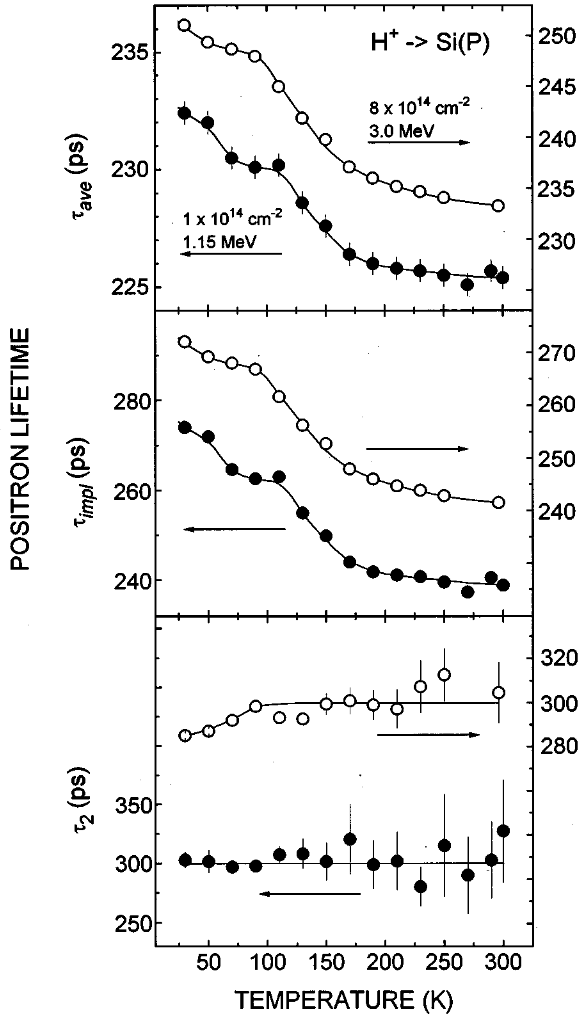

FIG. 3. Average positron lifetime τ_{ave}, positron lifetime τ_{impl} in the proton-implanted region, and the second component τ_2 of the three-component lifetime spectrum vs measurement temperature in unetched proton-implanted n-type Si: (●) sample $H2$, 1.15 MeV, 1×10^{14} cm^{-2} and (○) sample $H4$, 3.0 MeV, 8×10^{14} cm^{-2}. The solid lines are guides to the eye.

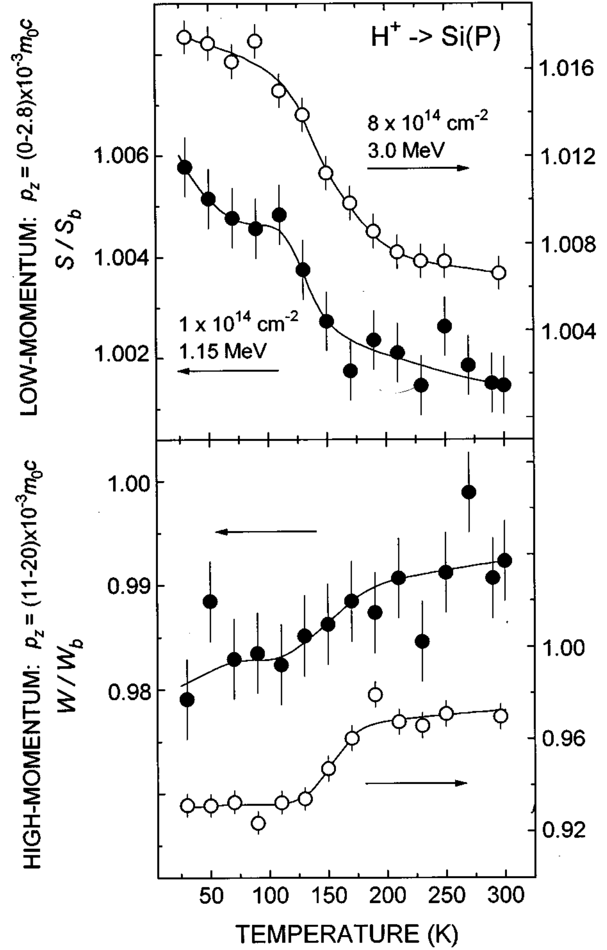

FIG. 4. S and W parameters of the Doppler-broadened annihilation line vs measurement temperature in unetched proton-implanted n-type Si: (●) sample $H2$, 1.15 MeV, 1×10^{14} cm^{-2} and (○) sample $H4$, 3.0 MeV, 8×10^{14} cm^{-2}. The solid lines are guides to the eye.

$H3$ is constant $\tau_2=(300\pm20)$ ps at 110–300 K and decreases from 300 to 280 ps as temperature decreases from 110 to 30 K.

In layer $A2$ (1.15 MeV, 20 μm, 1×10^{14} cm^{-2}) annealed at 400 °C only one component could be fitted in the positron lifetime spectra at 30–300 K. The positron lifetime shows still some temperature dependence and the difference to the value in as-grown n-type Si increases with decreasing temperature: $\tau_{\text{ave}}-\tau_{\text{ref}}<0.3$ ps at 300 K, $\tau_{\text{ave}}-\tau_{\text{ref}}=1$ ps at 110 K, and $\tau_{\text{ave}}-\tau_{\text{ref}}=2$ ps at 30 K.

2. Doppler-broadening measurements

In the as-grown n-type Si layer $R2$ the S parameter increases slightly and the W parameter decreases slightly as temperature increases from 30 to 300 K.

Figure 4 shows that in the proton-implanted layers $H2$ (1.15 MeV, 20 μm, 1×10^{14} cm^{-2}) and $H4$ (3.0 MeV, 90 μm, 8×10^{14} cm^{-2}) the S parameter is clearly higher and the W parameter is clearly lower than the corresponding values in as-grown n-type Si at 30–300 K. The temperature dependences of S and W are qualitatively similar to that found for the average positron lifetime. Layer $H3$ was not subjected to Doppler-broadening measurements.

In layer $A2$ (1.15 MeV, 20 μm, 1×10^{14} cm^{-2}) annealed at 400 °C the S and W parameters are close to the corresponding values in as-grown n-type Si. The S parameter increases slightly and the W parameter decreases slightly as temperature decreases from 300 to 30 K.

C. Spreading resistance measurements at 300 K

The spreading resistance results at 300 K are presented as a ratio $\rho/\rho_{\text{ref}}=(\mu_n n)/(\mu_{n,\text{ref}}n_{\text{ref}})$. Here ρ, μ_n and n are, respectively, the resistivity, the electron mobility, and the free-electron concentration in the proton-implanted layer, and ρ_{ref}, $\mu_{n,\text{ref}}$, and n_{ref} are the corresponding values in the as-grown layer $R5$.

The spreading resistance profile of the proton-implanted layer $H5$ (1.15 MeV, 20 μm, 1×10^{14} cm^{-2}) in Fig. 7(c) shows that the resistivity has increased after proton implantation. At depths 0–16 μm the resistivity of the implanted layer is 50–$100\rho_{\text{ref}}$. At 16–18 μm there is a peak in the

resistivity. Behind the peak the resistivity decreases again and reaches the reference level at about 24 μm.

In layer $A5$ annealed at 400 °C, the spreading resistance shows strong spatial variations, as seen in Fig. 7(d). At the surface the resistivity is almost the same as in the as-grown layer. At depths 4–15 μm the resistivity is much higher than in the as-grown layer. At 15–21 μm we observe a region where the resistivity is lower than in the as-grown layer, the lowest value being 0.1 ρ_{ref} at 17–18 μm. At depths >21 μm the resistivity is the same as in the as-grown layer.

IV. DEFECTS IN AS-IMPLANTED LAYERS

In this section we identify the different positron annihilation states in the n-type Si layers, before and after proton implantation.

A. Defect annihilation characteristics τ_d, S_d, and W_d

1. Before implantation

In the as-grown n-type Si layer $R2$, the positron lifetime 221–222 ps is close to the positron lifetimes 219–221 and 217–218 ps found earlier in silicon lattice.[20,21] The small linear temperature dependences of the positron lifetime, S parameter, and W parameter can be attributed to the thermal expansion of the silicon lattice. Also the diffusion length (220±10) nm at 300 K in layers $R1_{a-d}$ is in good agreement with the diffusion length 220 nm in bulk silicon at 300 K obtained from the work of Soininen *et al.*[16] Therefore, we conclude that in the as-grown n-type Si layers positrons annihilate mainly in the free-annihilation state in silicon lattice and the values τ_{ref}, S_{ref}, and W_{ref} correspond to the values τ_b, S_b, and W_b in silicon lattice.

2. After implantation

In the 1.15-MeV (20 μm) proton-implanted layers $H1_{a-i}$ and $H2$ and in the 3.0-MeV (90 μm) proton-implanted layers $H3$ and $H4$, the results $\tau_{\mathrm{ave}}>\tau_b$, $S>S_b$, and $W<W_b$ shown above indicate that positrons are trapped at vacancy-type defects. In layers $H2$, $H3$, and $H4$ we have determined a second lifetime component $\tau_2=(300\pm5)$ ps. To decide whether there are more than one type of positron traps present, we calculated a so-called model lifetime[5] $\tau_{\mathrm{mod}}=[(I_1/\tau_1+I_2/\tau_2)/(I_1+I_2)]^{-1}$ from the two positron lifetime components used in the implanted regions in layers $H2$, $H3$, and $H4$. If only one type of positron traps exists, we should find $\tau_{\mathrm{mod}}=\tau_b$. The presence of more than one type of traps is manifested as $\tau_{\mathrm{mod}}>\tau_b$. In the temperature range 110–300 K we found in layers $H2$, $H3$, and $H4$ that τ_{mod}=225–230 ps$\approx\tau_b$. As temperature decreases below 110 K, τ_{mod} increases strongly and is 250–255 ps$>\tau_b$ at 30 K. The same behavior of τ_{mod} is expected also in layers $H1_{a-i}$, because their proton implantation conditions are nominally identical to those of layer $H2$.

The findings above bring us to the conclusion that in the 1.15-MeV (20 μm) proton-implanted layers $H1_{a-i}$ and $H2$ and in the 3.0-MeV (90 μm) proton-implanted layers $H3$ and $H4$ the dominant positron trap at temperatures 110–300 K is a vacancy defect with a characteristic positron lifetime $\tau_d=(300\pm5)$ ps. Below 110 K there seems to be present another positron trap, the characteristic positron lifetime of that is lower than 300 ps. Hereafter, we shall concentrate on the characterization of the 300-ps defect, because it is the dominant positron trap at 300 K, at which temperature the depth profiling experiments with slow positrons and spreading resistance were performed.

We can use another method to check that the 300-ps defect is the dominant positron trap in the proton-implanted layers. Any of the three mean annihilation quantities $F^i\in[F^1=\tau_{\mathrm{ave}},\ F^2=S,\ F^3=W]$ can be expressed as a superposition of annihilations states:

$$F^i=\eta_bF_b^i+\sum_j^N\eta_{dj}F_{dj}^i\quad\text{with}\quad\eta_b+\sum_j^N\eta_{dj}=1,\tag{5}$$

where the subscript b corresponds to the free annihilation state in the lattice, the subscripts $dj=d1,\ d2,\ldots,dN$ correspond to N defect states, and η_b and η_{dj} are the fractions of positrons annihilating in the corresponding states. When only one defect is acting as a positron trap, Eq. (5) is reduced to two terms $F^i=\eta_bF_b^i+\eta_dF_d^i$. Then $S(\tau)$, $W(\tau)$, and $S(W)$ are linear functions. Figure 5 shows that the $S(\tau)$ and $W(\tau)$ curves for the proton-implanted layers $H2$ (1.15 MeV, 20 μm, 1×10^{14} cm^{-2}) and $H4$ (3.0 MeV, 90 μm, 8×10^{14} cm^{-2}) are straight lines. This indicates that the data follow the one-trap model very well. Below 110 K the $S(\tau)$ and $W(\tau)$ curves deviate only slightly from the straight lines.

We determine the characteristic momentum parameters S_d and W_d of the 300-ps defect as follows. By extrapolating the lines $S(\tau)$ and $W(\tau)$ in Fig. 5 to the positron lifetime τ_d=300 ps at the vacancy defect, we obtain its characteristic S and W parameters as $S_d=(1.052\pm0.003)S_b$ and $W_d=(0.78\pm0.02)W_b$, respectively.

B. Positron trapping rate to the τ_d=300 ps defect

We can follow the changes in the concentration c_d of the vacancy defect in the proton-implanted layers by calculating the positron trapping rate to the vacancies $\kappa_d=\mu_dc_d$, where μ_d is the trapping coefficient. When there is only one type of defect acting as a positron trap in the implanted region, the positron trapping rate κ_d to the defect can be calculated as[5]

$$\kappa_d=\frac{F_{\mathrm{impl}}^i-F_b^i}{F_d^i-F_{\mathrm{impl}}^i}\,\tau_b^{-1},\tag{6}$$

where the annihilation quantities F^i (i=1,2,3) are as in Eq. (5).

1. Unetched n-type Si layers implanted with 1.15-MeV (20 μm) and 3.0-MeV (90 μm) protons

Figure 6 shows the temperature dependence of the positron trapping rate κ_d to the τ_d=300 ps defect in the unetched proton-implanted layers $H2$ (1.15 MeV, 20 μm, 1×10^{14} cm^{-2}) and $H4$ (3.0 MeV, 90 μm, 8×10^{14} cm^{-2}). The trapping rate has been calculated by using the positron lifetimes τ_{impl} of Fig. 3 in Eq. (6). The solid lines indicate the temperature behavior of κ_d assuming that $\kappa_d\propto T^{-n}$. We see that n=0.5 at 190–300 K and n=2 at 110–170 K. In layer $H3$ we obtain the same values of n as in layers $H2$ and

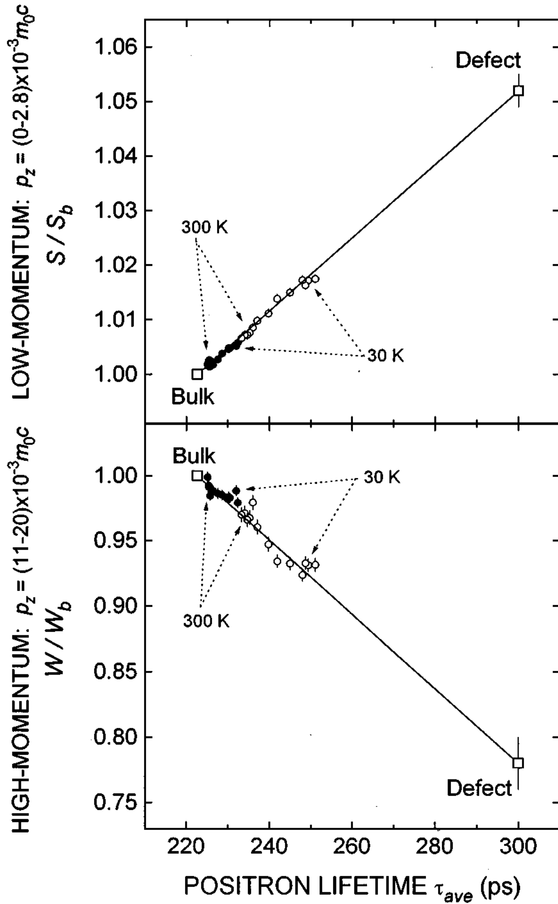

FIG. 5. Determination of the characteristic S_d and W_d parameters at the defect corresponding to a positron lifetime 300 ps in unetched proton-implanted n-type Si. The data of Fig. 4 have been plotted vs the data of Fig. 3: (●) sample $H2$, 1.15 MeV, 1×10^{14} cm^{-2} and (○) sample $H4$, 3.0 MeV 8×10^{14} cm^{-2}. The solid lines are fits of the two-state trapping model in the data. The symbols (□) correspond to the bulk silicon and to the defect extrapolated at 300 ps.

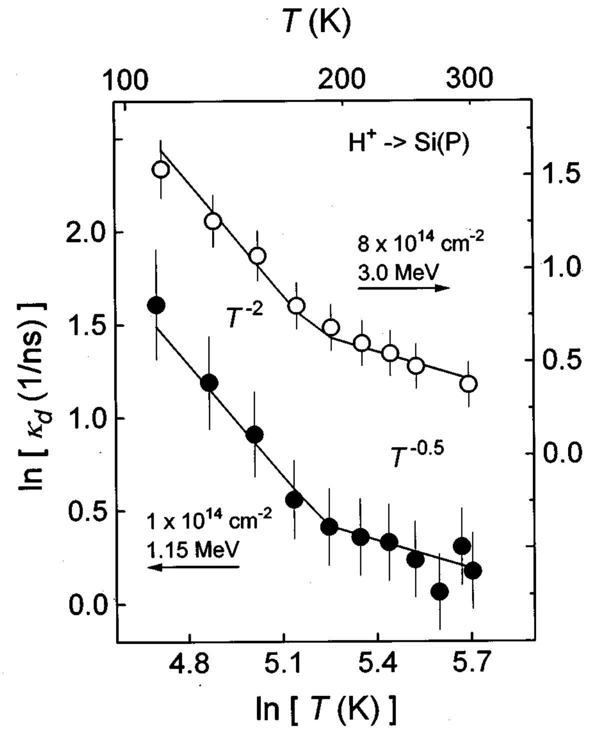

FIG. 6. Temperature dependence of the positron trapping rate κ_d to the 300 ps defect calculated from the positron lifetime data of Fig. 3, in unetched proton-implanted n-type Si: (●) sample $H2$, 1.15 MeV, 1×10^{14} cm^{-2} and (○) sample $H4$, 3.0 MeV, 8×10^{14} cm^{-2}.

$H4$, the values of κ_d being 0.5 ns^{-1} at 300 K, 0.7 ns^{-1} at 190 K, and 1.6 ns^{-1} at 110 K.

2. Etched n-type Si layers implanted with 1.15-MeV (20 μm) protons

The positron trapping rate κ_d at 300 K to the 300-ps defect in the etched layers $H1_{a-i}$ (1.15 MeV, 20 μm, 1×10^{14} cm^{-2}) is calculated by inserting the slow-positron data of Fig. 2 in Eq. (6). We use the defect specific values $S_d=(1.052\pm0.003)S_b$ and $W_d=(0.78\pm0.02)W_b$ determined above from the fast-positron results. The κ_d profiles obtained from the S and W results are found to be almost identical, which indicates that one vacancy-type defect is observed at all etched depths at 300 K. An average of the two κ_d profiles, weighted by the inverse errors of the data points, is presented in Fig. 7(a).

3. Comparison between etched and unetched n-type Si layers implanted with 1.15-MeV (20 μm) protons

By comparing the results of the slow-positron and the fast-positron measurements in the etched layers $H1_{a-i}$ (1.15 MeV, 20 μm, 1×10^{14} cm^{-2}) and in the unetched layer $H2$ (1.15 MeV, 20 μm, 1×10^{14} cm^{-2}) proton implanted nominally in the same conditions, we can check whether the two methods give similar positron trapping rates. In Fig. 7(a) we see that the trapping rate in layers $H1_{a-i}$ determined with slow-positron measurements is on the average $\kappa_d=0.4$ ns^{-1} at depths 0–25 μm. In layer $H2$ we obtained a somewhat higher value 1.1 ns^{-1} at 300 K with positron lifetime measurements, as can be calculated from Fig. 6. These values are of the same order of magnitude. The value of κ_d in the unetched layer $H2$ is, however, about three times higher than the mean value of κ_d in the etched layers $H1_{a-i}$.

A difference in κ_d can be introduced by disregarding in the positron lifetime analysis the inhomogeneity of the vacancy distribution at depths 0–25 μm. A bigger systematic error in the determination of κ_d from the positron lifetime data can also come from calculating the fraction I_{ref} of positrons annihilating in the bulk behind the vacancy distribution. A change in I_{ref} by 50% from 80% to 40%, which corresponds to reducing of the fast-positron penetration depth $1/\alpha$ from 110 to 50 μm yields nearly the same values of 0.6 and 0.5 ns^{-1} by the fast-positron and the slow-positron methods, respectively. This effects only little the characteristic annihilation parameters of the defect: τ_d changes by 3% from 300 to 290 ps, S_d by 0.6% from $1.052S_b$ to $1.045S_b$, and W_d by 4% from $0.78W_b$ to $0.81W_b$. Hence, the positron trapping rate 1.1 ns^{-1} calculated from the positron lifetime data could be too high because of too high I_{ref}. The positron trapping rate κ_d

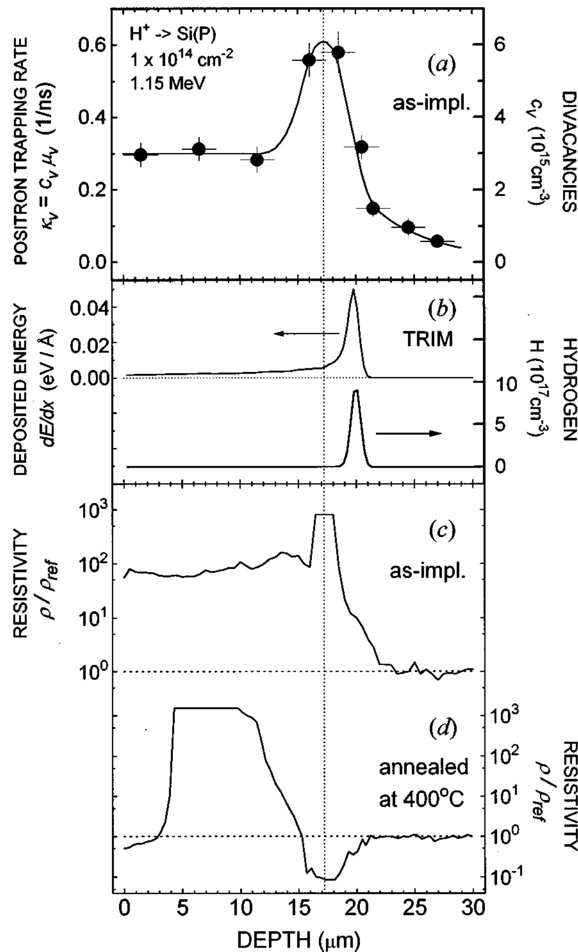

FIG. 7. Comparison of vacancy, hydrogen, and resistivity profiles in Si implanted with 1.15-MeV protons to a dose $1\times10^{14}\ \mathrm{cm}^{-2}$: (a) positron trapping rate at 300 K to the 300-ps vacancy after implantation (samples $H1_{a-i}$), (b) distributions of hydrogen after implantation and the energy deposited in nuclear collisions obtained with a TRIM simulation, (c) spreading resistance at 300 K after implantation (sample $H5$), and (d) spreading resistance at 300 K after implantation and subsequent annealing at 400 °C (sample $A5$).

$=0.4-0.5\ \mathrm{ns}^{-1}$ calculated from the slow-positron data is more accurate. Finally, as the proton implantations were performed at three different runs, the conditions may have changed slightly from one run to another.

C. Properties of the defects

In the following, we discuss the properties and the identification of the $\tau_d=300$ ps defect.

1. Silicon divacancy V_2

The dominant positron trap at 110–300 K in 1.15- and 3.0- MeV proton-implanted n-type Si has the following characteristic annihilation parameters: $\tau_d=(300\pm5)$ ps $=1.35\tau_b$, $S_d=(1.052\pm0.003)S_b$, and $W_d=(0.78\pm0.02)W_b$. We identify this defect as the silicon divacancy V_2 on the basis of the following arguments.

(i) The positron lifetime at the defect $\tau_d=(300\pm5)$ ps is close to the theoretical value 309 ps at the divacancy calculated by Puska *et al.*[22]

(ii) The positron lifetime $\tau_d=(300\pm5)$ ps$=1.35\tau_b$ is higher than experimentally determined positron lifetimes at monovacancy defects in silicon: $\tau_d(V-P)=250$ ps$=1.14\tau_b$ and $\tau_d(V_{\mathrm{Si}})=270\ ps=1.23\tau_b$.[20] The high-momentum parameter $S_d=(1.052\pm0.003)S_b$ is also clearly higher than the values reported for monovacancy defects in other semiconductors: e.g., $S_d(V_{\mathrm{Ga}})=1.027S_b$ in GaAs.[23]

The positron annihilation results are in agreement with electron paramagnetic resonance (EPR) measurements in electron-irradiated silicon, according to which the most abundant point defect existing in low-impurity silicon after irradiation and room temperature annealing is the divacancy V_2.[24] In electron-irradiated float-zone silicon Avalos and Dannefaer[25] have assigned a positron lifetime of (290±5) ps to divacancies, which is in rather good agreement with the value (300±5) ps that we attribute to divacancies in proton-implanted CVD-grown silicon. They also gave a value $(1.067\pm0.002)S_b$ for the characteristic S parameter for the divacancy, which is slightly higher than the value $(1.052\pm0.003)S_b$ determined in this work.

Below 110 K the one-trap model is not valid. This indicates that at temperatures <110 K at least one other defect acts as a positron trap and for this defect $\tau_d<300$ ps. Potential candidates are small concentrations of monovacancy-type defects such as V-P (Ref. 20) or V_2-O (Ref. 11) or so-called shallow positron traps such as V-O (Ref. 26). As positron trapping to this other trap is not observed at 300 K where our main interest is, hereafter we shall consider only the divacancy.

After proton implantation the silicon layers are highly resistive and the position of the Fermi level E_f is expected to be rather insensitive to the temperature between 30–300 K. We can assume that as temperature decreases, the concentration c_v of the divacancies remains in the same charge state as at 300 K. The temperature dependence of the positron trapping rate $\kappa_v=\mu_v c_v$ to the divacancy can be ascribed to the positron trapping coefficient μ_v to the divacancy. Above we observed that $\kappa_v\propto T^{-0.5}$ at 190–300 K and $\kappa_v\propto T^{-2}$ at 110–170 K. According to Puska and co-workers[6,27] the positron trapping coefficient μ_v to the ground state of a negative vacancy is proportional to $T^{-0.5}$. As temperature decreases, the positron can get trapped at a shallow Rydberg state around the vacancy and the trapping coefficient μ_v is proportional to T^{-n}, where $n>1$. The positron-trapping coefficient to a neutral vacancy does not depend on temperature. We have thus observed the temperature dependence theoretically expected for a negative vacancy. Furthermore, this agreement between theory and experiment validates our assumption that the divacancies remain in the same charge state as temperature decreases from 300 to 110 K. We conclude that the divacancy in the proton-implanted n-type Si is in a negative charge state.

The divacancy is known to have three ionization levels $V_2^{2-/-}$, $V_2^{-/0}$, and $V_2^{0/+}$ in the band gap of silicon. EPR measurements of Watkins and Corbett[28] indicate a position in the band gap for two of the electronic levels of the divacancy: $V_2^{2-/-}$ at $E_c-0.40$ eV and $V_2^{0/+}$ at $E_v+0.23$ eV. Photoconductivity measurements of Kalma and Corelli[29] and Young and Corelli[30] suggest that the $V_2^{-/0}$ level is at $E_c-0.54$ eV. Another scheme for the two acceptor levels is

given by Evwaraye and Sun[31] on the basis of their DLTS measurements: $V_2^{2-/-}$ at $E_c-0.23$ eV and $V_2^{-/0}$ at $E_c-0.40$ eV.

To decide whether the negative divacancy observed with positron annihilation in proton-implanted n-type Si is V_2^- or V_2^2 we estimate the Fermi-level position E_f in the implanted layers. Under the assumption that the effect of the proton implantation on the electron mobility is small, the free-electron concentrations n in the proton-implanted layers $H1_{a-i}$, $H2$, and $H5$ (1.15 MeV, 20 μm 1×10^{14} cm^{-2}) can be estimated from the spreading resistance results. From Fig. 7(c) we find that $n=1-5\times10^{12}$ cm^{-3} at depths 0–16 μm and $n=1\times10^{11}-1\times10^{12}$ cm^{-3} at depths 16–18 μm. The Fermi-level positions at the corresponding depths are then $E_c-E_f=0.40-0.45$ eV and $E_c-E_f=0.45-0.55$ eV, respectively.[32] The positron annihilation results seem to be in accordance with the level assignments $V_2^{2-/-}$ at $E_c-0.40$ eV and $V_2^{-/0}$ at $E_c-0.54$ eV based on EPR and photoconductivity measurements. We conclude that in the 1.15-MeV proton-implanted n-type Si layers the divacancy is dominantly in the singly negative charge state V_2^-.

The divacancy concentration in the proton-implanted layers $H1_{a-i}$ (1.15 MeV, 20 μm 1×10^{14} cm^{-2}) in Fig. 7(a) can now be estimated. According to Mascher, Dannaefer, and Kerr[26] the positron-trapping coefficient to V_2^- at 300 K in electron-irradiated Si is $\mu_v=4\times10^{15}$ s^{-1}. Another estimate given by Kawasuo *et al.*[33] is $\mu_v=1\times10^{16}$ s^{-1}. Using both values of μ_v we obtain the divacancy concentrations $[V_2^-]=2-4\times10^{15}$ cm^{-3} at depths 0–14 μm along the track of the proton and $[V_2^-]=4-8\times10^{15}$ cm^{-3} at depths 16–18 μm near the proton stopping range.

2. *Defect profiles*

By comparing the divacancy profile of Fig. 7(a) with the resistivity profile of Fig. 7(c) we notice that the resistivity increases with the divacancy concentration. The electronic compensation is due to trapping of free carriers at deep electron levels such as those of the divacancy. The concentration estimates $[V_2^-]\sim10^{15}-10^{16}$ cm^{-3} given above suggest that the divacancies compensate not only the phosphorus donors $[P]=1\times10^{14}$ cm^{-3} but also another positively charged species induced by the proton implantation.

To obtain theoretical estimates for the hydrogen and vacancy profiles induced by the proton implantation, we performed simulations of 1.15- and 3.0-MeV proton implantations in Si with TRIM v 95.[34] The TRIM code contains only ballistic processes and not, for example, diffusion of defects and hydrogen in the lattice. Therefore the stragglings of the simulated hydrogen and vacancy distributions are probably smaller than in reality. In the upper part of Fig. 7(b) we show the profile of the energy deposited in nuclear collisions in 1.15-MeV proton implantation. In TRIM this profile is proportional to the distribution of implantation-induced vacancies. Along the track of the proton, at depths 0–15 μm, the deposited energy is $2-4\times10^{-3}$ eV/Å. The strong increase of the deposited energy towards the end of the proton track reflects the energy-dependent cross section of nuclear collisions in TRIM. In the lower part of Fig. 7(b) we show the hydrogen profile after 1.15-MeV proton implantation to a dose 1×10^{14} cm^{-2}. The maximum hydrogen concentration to be expected at any depth after implantation is 9×10^{17} cm^{-3}. In the simulation of 3.0-MeV proton implantation in silicon the peaks of the hydrogen and deposited energy distributions are found at depth 90 μm. Along the track of the proton, at depths 0–80 μm, the deposited energy is $(1-2)\times10^{-3}$ eV/Å.

The measured divacancy profile in Fig. 7(a) looks qualitatively similar to the calculated deposited-energy profile in Fig. 7(b), but two differences can be observed. First, the peak in the divacancy concentration occurs 3 μm before the peak in the deposited energy profile. Second, the peak in the divacancy profile is broader than the peak in the simulated deposited energy profile. We suggest for the difference between experiment and theory the following reasons.

(i) In the region near the proton stopping range the hydrogen can be trapped at vacancy defects. As observed previously by positron annihilation measurements in GaAs (Ref. 23) and in Si,[8,9] the occupation of vacancies by hydrogen may prevent positron trapping, which can be reactivated only in thermal annealing when hydrogen is released from the vacancies. The decoration of vacancies by hydrogen can mask the vacancy distribution from positrons in the region of the peak in the deposited-energy distribution that is close to the peak in the hydrogen distribution.

(ii) The defects introduced by the proton implantation diffuse and anneal out during the implantation process. This results in a broadening of the vacancy profile.

The effect of the proton-implantation energy on the observed positron-trapping rates is considered as follows. Layers $H2$ and $H3$ are implanted to the same proton dose 1×10^{14} cm^{-2} with different proton energies 1.15 and 3.0 MeV, respectively. The ratio of the positron trapping rates to divacancies at 300 K in the two layers is $\kappa_v(H2)/\kappa_v(H3)\approx2$. This experimental value is in agreement with the value calculated with the TRIM simulations: the energy deposited in nuclear collisions and the induced vacancy concentration along the track of the proton is two times higher in the 1.15-MeV proton implantation than in the 3.0-MeV proton implantation.

Finally, we discuss the effect of the proton implantation dose on the observed positron trapping rates. Layers $H4$ and $H3$ are implanted with the same proton energy 3.0 MeV to different doses 8×10^{14} and 1×10^{14} cm^{-2}, respectively. The ratio of the positron trapping rates to divacancies at 300 K in the two layers is $\kappa_v(H4)/\kappa_v(H3)=3$, which is clearly smaller than the ratio 8 of the implantation doses. The difference can be understood as a consequence of the diffusion and annealing of the defects during the implantation process. This is also in agreement with the idea that the divacancy profile is broadened due to the diffusion of defects.

V. DEFECTS IN ANNEALED LAYERS

The changes in the divacancy concentration and in the divacancy and resistivity profiles induced by the annealing at 400 °C are discussed in the following.

A. Positron trapping at vacancies

In layer $A2$ (1.15 MeV, 20 μm, 1×10^{14} cm^{-2}) annealed at 400 °C the positron lifetime increases slightly as tempera-

ture decreases, which reveals the presence of a small concentration of negative vacancies. At 300 K the positron trapping at vacancies is below the detection limit and we cannot obtain a vacancy profile by slow-positron measurements. The positron lifetime results allow us to make an estimate of the vacancy concentration remaining after the annealing by assuming that the width of the defected region and the nature of the dominant positron trap are the same as in the as-implanted material. In layer $A2$ the width of the defected region is then 25 μm and the defect specific annihilation parameters are $\tau_d=(300\pm5)$ ps, $S_d=(1.052\pm0.003)S_b$, and $W_d=(0.78\pm0.02)W_b$. Carrying out the same procedure as for the as-implanted layers with the above-mentioned assumptions, yields a positron trapping rate 0.05–0.1 ns^{-1} to the 300 ps defect at 300 K. Using the values of μ_v given above for the divacancy, we can estimate that the concentration of negative vacancy-type defects remaining after the 400 °C annealing is equivalent to a divacancy concentration of 10^{14} cm^{-3}.

The concentration of divacancies after thermal annealing at 400 °C is much lower than in the as-implanted layer. The decrease of the vacancy concentration throughout the implanted region is most likely due to the annealing of the divacancies. According to EPR measurements an annealing stage of divacancies is at 200–300 °C.[24]

B. Role of vacancies in the resistivity profile

1. Acceptors

At depths 4–15 μm in the annealed layer $A5$ in Fig. 7(d) the resistivity remains high after annealing, which indicates a compensation by remaining defects. The positron annihilation results indicate that there are indeed negatively charged defects in concentration comparable to the phosphorus-donor concentration $[\text{P}]=1\times10^{14}$ cm^{-3}.

2. Shallow donors

At depths 15–21 and 0–3 μm in layer $A5$ (1.15 MeV, 20 μm 1×10^{14} cm^{-2}) annealed at 400 °C the resistivity decreases below the reference level. The low resistivity at 15–21 μm near the proton range is a well-known effect and it has been shown previously that it is due to the formation of shallow donors.[35] The maximum shallow-donor concentration at depths 16–18 μm is approximately 10^{15} cm^{-3}. The effect at 0–3 μm near the surface is less clear. It may be due to the passivation of the defects near the surface either by migrating impurities or because of the contamination of the irradiated surface during the annealing. In the following, we leave the surface resistivity as an open question and we discuss the shallow donors near the proton range.

It is generally agreed that the shallow donors induced in silicon by proton implantation and subsequent annealing at 300–500 °C involve hydrogen, but the microscopic configuration of the donors is not clear.[3,4] The IR absorption measurements of Mukashev *et al.*[36] in proton-implanted silicon suggest that the shallow donors are divacancy-hydrogen complexes V_2-4H.

In Figs. 7(d) and 7(a) we see that the spatial profile of the shallow donors after annealing occurs exactly at the same depth as the peak in the divacancy profile before annealing, which suggests that divacancies play a role in the formation of the hydrogen-related donors. We notice also that the maximum shallow-donor concentration is only $(10^{15}\ \text{cm}^{-3})/(10^{17}\ \text{cm}^{-3})=1\%$ of the maximum hydrogen concentration, which indicates that something else than the hydrogen concentration is limiting the formation of the hydrogen-related donors. Supposing that the donors were hydrogen-vacancy complexes, the limiting factor would be the vacancy concentration before annealing. In our case the maximum divacancy concentration before annealing is $4-8\times10^{15}$ cm^{-3}, which is indeed close to the measured shallow-donor concentration. We conclude that the positron annihilation and the spreading resistance results support the idea that the shallow donors formed in silicon by proton implantation and subsequent thermal annealing are hydrogen-vacancy complexes.

We have also proposed the decoration of vacancies by hydrogen in the hydrogen peak region in the as-implanted material, but there no shallow donors were observed. This would suggest that the nature of the hydrogen-vacancy complexes formed directly in the proton implantation is different from that of the shallow hydrogen-related donors observed after annealing.

VI. CONCLUSIONS

To elucidate the nature and profile of vacancy-type defects after proton implantation in n-type Si(P) layers we have performed positron-electron pair momentum-distribution measurements with a slow-positron beam carried out as a function of etching depth, and e^+-e^- pair momentum-distribution and positron lifetime measurements in unetched layers with a ^{22}Na source. Momentum distributions were measured with the Doppler-broadening technique. We have also compared the vacancy profile with the resistivity profile measured with the spreading resistance technique.

The dominant positron trap induced by 1.15 and 3.0 MeV proton implantations is the silicon divacancy V_2. The characteristic positron lifetime at the divacancy is $\tau_d=(300\pm5)$ ps$=1.35\tau_b$. The characteristic low-momentum [for $p_z=(0-2.8)\times10^{-3}m_0c$] and high-momentum [for $p_z=(11-20)\times10^{-3}m_0c$] parameters of the e^+-e^- pair momentum distribution at the divacancy are $S_d=(1.052\pm0.003)S_b$ and $W_d=(0.78\pm0.02)W_b$, respectively. The divacancy is observed in the negative charge state V_2^-.

The divacancy profile is measured in n-type Si implanted with 1.15-MeV (20 μm) protons to a dose 1×10^{14} cm^{-2}. The divacancy concentration is $[V_2^-]=2-4\times10^{15}$ cm^{-3} at depths 0–14 μm. The maximum concentration $[V_2^-]=4-8\times10^{15}$ cm^{-3} is observed at 16–18 μm. The resistivity increases with increasing divacancy concentration. The peak in the divacancy profile is broader and shifted towards the surface in comparison with the profile of deposited energy calculated with TRIM. This is attributed to the formation of hydrogen-vacancy complexes near the proton range and to the diffusion and annealing of defects during the implantation.

After annealing at 400 °C the remaining negative vacancy concentration is of the order of 10^{14} cm^{-3}. Spreading resistance measurements reveal a region of shallow hydrogen-

related donors at depths 15–21 μm. The shallow-donor concentration 10^{15} cm^{-3} is much lower than the maximum hydrogen concentration. The spatial profile of the shallow donors overlaps perfectly with the peak of the divacancy profile observed before annealing. The shallow-donor concentration is also close to the maximum divacancy concentration observed before annealing. This result supports the idea that the introduction of shallow donors is due to the formation of new hydrogen-vacancy complexes during the annealing at 400 °C.

[1] D. C. Sawko and J. Bartko, IEEE Trans. Nucl. Sci. **NS-30**, 1756 (1983).

[2] M. W. Hüppi, J. Appl. Phys. **68**, 2702 (1990).

[3] S. M. Myers, M. I. Baskes, H. K. Birnbaum, J. W. Corbett, G. G. DeLeo, S. K. Estreicher, E. E. Haller, P. Jena, N. M. Johnson, R. Kircheim, S. J. Pearton, and M. J. Stavola, Rev. Mod. Phys. **64**, 559 (1992), especially p. 583, and references therein.

[4] S. J. Pearton, J. W. Corbett, and T. S. Shi, Appl. Phys. A **43**, 153 (1987), especially pp. 175 and 181, and references therein.

[5] P. Hautojärvi and C. Corbel, in *Positron Spectroscopy of Solids*, edited by A. Dupasquier and A. P. Mills, Jr. (IOS, Amsterdam, 1995), pp. 491 and 533.

[6] M. J. Puska and R. M. Nieminen, Rev. Mod. Phys. **66**, 641 (1994).

[7] P. Asoka-Kumar, K. G. Lynn, and D. O. Welch, J. Appl. Phys. **76**, 4935 (1994).

[8] R. S. Brusa, M. Duarte Naia, A. Zecca, C. Nobili, G. Ottaviani, R. Tonini, and A. Dupasquier, Phys. Rev. B **49**, 7271 (1994).

[9] J. Keinonen, M. Hautala, E. Rauhala, M. Erola, J. Lahtinen, H. Huomo, A. Vehanen, and P. Hautojärvi, Phys. Rev. B **36**, 1344 (1987); J. Keinonen, M. Hautala, E. Rauhala, V. Karttunen, A. Kuronen, J. Räisänen, J. Lahtinen, A. Vehanen, E. Punkka, and P. Hautojärvi, *ibid*. **37**, 8269 (1988).

[10] R. D. Goldberg, P. J. Schultz, and P. J. Simpson, Appl. Surf. Sci. **85**, 287 (1995).

[11] S. Mäkinen, H. Rajainmäki, and S. Linderoth, Phys. Rev. B **42**, 11 166 (1990).

[12] S. Mäkinen, H. Rajainmäki, and S. Linderoth, Phys. Rev. B **44**, 5510 (1991).

[13] K. G. Lynn, D. M. Chen, B. Nielsen, R. Pareja, and S. Myers, Phys. Rev. B **34**, 1449 (1986).

[14] S. Valkealahti and R. M. Nieminen, Appl. Phys. A **35**, 51 (1984).

[15] R. M. Nieminen and J. Oliva, Phys. Rev. B **22**, 2226 (1980).

[16] E. Soininen, J. Mäkinen, D. Beyer, and P. Hautojärvi, Phys. Rev. B **46**, 13 104 (1992).

[17] J. Gebauer, S. Eichler, R. Krause-Rehberg, and H. P. Zeindl (unpublished).

[18] A. van Veen, H. Schut, J. de Vries, R. A. Hakvoort, and M. R. Ijpma, in *Positron Beams for Solids and Surfaces*, edited by P. J. Schultz, G. R. Massoumi, and P. J. Simpson, AIP Conf. Proc. No. 218 (AIP, New York, 1990), p. 171.

[19] R. Paulin, in *Positron Solid-State Physics*, edited by W. Brandt and A. Dupasquier (North-Holland, Amsterdam, 1983), p. 565.

[20] J. Mäkinen, C. Corbel, P. Hautojärvi, P. Moser, and F. Pierre, Phys. Rev. B **39**, 10 162 (1989).

[21] J. Mäkinen, P. Hautojärvi, and C. Corbel, J. Phys. Condens. Matter **4**, 5137 (1992).

[22] M. J. Puska, S. Mäkinen, M. Manninen, and R. M. Nieminen, Phys. Rev. B **39**, 7666 (1989).

[23] K. Saarinen, P. Hautojärvi, J. Keinonen, E. Rauhala, J. Räisänen, and C. Corbel, Phys. Rev. B **43**, 4249 (1991).

[24] G. D. Watkins, in *Deep Centers in Semiconductors*, edited by S. T. Pantelides (Gordon and Breach, New York, 1986), p. 147.

[25] V. Avalos and S. Dannefaer, Phys. Rev. B **54**, 1724 (1996).

[26] P. Mascher, S. Dannaefer, and D. Kerr, Phys. Rev. B **40**, 11 764 (1989).

[27] M. J. Puska, C. Corbel, and R. M. Nieminen, Phys. Rev. B **41**, 9980 (1990).

[28] G. D. Watkins and J. W. Corbett, Phys. Rev. **138**, A543 (1965).

[29] A. H. Kalma and J. C. Corelli, Phys. Rev. **173**, 735 (1968).

[30] R. C. Young and J. C. Corelli, Phys. Rev. B **5**, 1455 (1972).

[31] A. O. Evwaraye and E. Sun, J. Appl. Phys. **47**, 3776 (1976).

[32] S. M. Sze, *Physics of Semiconductor Devices*, 2nd ed. (Wiley, New York, 1981), p. 26.

[33] A. Kawasuo, M. Hasegawa, M. Suezawa, S. Yamaguchi, and K. Sumino, Jpn. J. Appl. Phys. **34**, 2197 (1995).

[34] J. F. Ziegler, J. P. Biersack, and U. Littmark, *The Stopping and Ranges of Ions in Matter*, edited by J. F. Ziegler (Pergamon, New York, 1985), Vol. 1, pp. 109 and 183.

[35] E. Ntsoenzok, J. F. Barbot, P. Desgardin, J. Vernois, C. Blanchard, and D. B. Isabelle, IEEE Trans. Nucl. Sci. **41**, 1932 (1994).

[36] B. Mukashev, S. Tokmoldin, and M. Tamendarov, S. Tokmoldin, B. Mukashev, M. Tamendrov, and S. Chasnikova, in *Defect Control in Semiconductors*, Proc. ICSTDS-89, edited by K. Sumino (North-Holland, Amsterdam, 1990), pp. 429 and 425.